Exploration of anti-corrosive activity of TP (thespesia populnea)-TiO$_2$ composite coating for mild steel (CS) in aggressive environments

Athira Krishnan[†]

Department of Chemistry, Amrita Vishwa Vidyapeetham, Amritapuri, 690525, India

Abstract−As part of promoting eco-friendly research & development, corrosion chemistry encourages green inhibitors for metal corrosion prevention. Thespesia Linoleic acid, n-Hexadecanoic acid, trans-Squalene, Phytol were identified as the active components responsible for corrosion inhibition. The optimum concentration of 500 ppm could deliver protection with efficiency in the range of 97%-98%. Additionally, we extended the study to evaluate the extract's capability for its use in the paint industry. The remarkable potential of the TiO$_2$-TP composite coating thus developed was illustrated by physico-chemical, electrochemical, and surface analyses. According to the electrochemical impedance spectroscopy (EIS) study, the applied leaf extract loaded coatings resist corrosion of CS at efficiencies of 97.9%, 91.6%, and 98.5% in 1 M HCl, 1 M HCl at 80 °C, and rainwater mediums, respectively. The proposed composite coating is undoubtedly promising for industrial application and is also recommended by green protocols.

Keywords: Green Inhibitor, Electrochemical Corrosion, Thespesia Populnea, TiO$_2$, Passive Film, Barrier Protection

INTRODUCTION

Corrosion of metals is a severe industrial issue, as leakage of machinery insists on immediate shutdown of plants, which will cause substantial economic loss [1]. Localized corrosion is often challenging to identify, comparable to uniform corrosion [2]. Among the metals, mild steels are extensively used in industries due to their superior mechanical properties and cost-effectiveness. Acid pickling is an established strategy used to remove surface impurities from metals. Acid pickling is often done with a solution consisting of strong acids. It may accelerate the corrosion of metals, but use of appropriate corrosion inhibitors could overcome this acid corrosion. Instead of using toxic synthetic compounds, our research community is now focused on developing and applying green corrosion inhibitors [3,4]. The first evidence of natural products used as corrosion inhibitors was in the 1930s. Since then, many reports have been published on green inhibitors protecting metals from acid pickling, aggressive water, acidified oil wells, cooling water system, etc. [5-7]. Highly toxic chromate, phosphate, and arsenic compounds, which once excelled as supreme corrosion inhibitors, are now outweighed by the so-called green corrosion inhibitors. Recently, there has been a tremendous increase in research on natural products such as plant extracts and essential oils aimed at developing environmentally-friendly corrosion inhibitors [8-15]. A corrosion inhibitor can protect metals or alloys at a very low concentration in an electrolytic medium. Plant extracts, a rich source of naturally synthesized chemical compounds, can significantly reduce the rate of corrosion by the adsorption of its active chemical constituents on the metal surface when added to a corrosive medium. The adsorbed species will deter metal corrosion by changing either the rate of anodic/cathodic reactions, altering the rate of diffusion of aggressive ions interacting with metallic species, or developing a protective barrier layer over the metal surface [16].

Thespesia populnea (TP) is an ever-green shrubby tree that belongs to the Malvaceae family. It is a flowering plant found worldwide, especially in coastal areas and is commonly known by Pacific rosewood and Indian tulip tree names. The plant has numerous medicinal applications [17]. The leaf extract is a rich source of alkaloids, proteins, amino acids, phenols, flavonoids, terpenes, tannins, etc., and is usually used to treat cough, influenza, headache, and chronic illness. The leaf sap is used externally for skin diseases. Different parts of this plant, such as leaf, bark, flower, and fruit, are proven for their medicinal uses, such as anti-inflammatory diseases and skin and liver diseases. Leaf extract of TP was found to possess anti-bacterial and anti-oxidant activities [18-20]. Herein, we investigated the corrosion inhibition activity of TP leaf extract, which was not ever discussed in the literature. In the study, ethanolic extract of TP leaves was evaluated for its corrosion inhibition activity of mild steel in a 1 M HCl medium.

To explore the industrial significance of TP leaf extract, we prepared a composite of it with TiO$_2$, the primary constituent used to impart white color and opacity in paint. The as-prepared composite is coated over mild steel, and its anti-corrosive performance is evaluated in HCl, HCl at 80 °C, and rainwater mediums. The observations are substantiated with advanced electrochemical, morphological, and spectroscopic techniques.

MATERIALS AND METHODS

1. Preparation of the Extract

Thespesia populnea leaves were collected from the premises of Amrita School of Arts and Sciences, Amritapuri, Kollam, Kerala.

[†]To whom correspondence should be addressed.
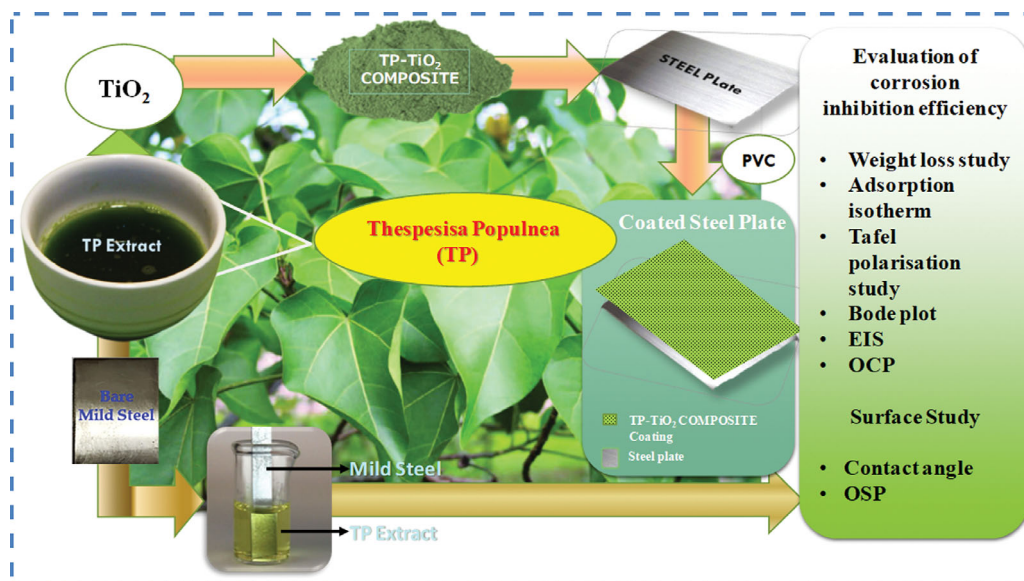E-mail: athikrishnan91@gmail.com

Fig. 1. Schematic representation of overall experimental study.

Leaves were then washed, dried in a mechanical convection oven at 100 °C, and ground to powder form. About 20 g of the powder was soaked in 99% ethanol in a 200 ml volumetric flask and allowed to stand for 48 h at room temperature. The soaked sample was filtered, kept in a magnetic stirrer for an hour and then excess solvent was removed by using rota-vapor. The dried residue was stored in a desiccator. 1 g of it, was dissolved in 1,000 mL of 1 M HCl and is taken as the bulk solution. It was then diluted to prepare concentrations such as 100 ppm, 200 ppm, 300 ppm and 500 ppm to evaluate its inhibitive action on the corrosion of mild steel coupons [9,21,22].

2. Pre-treatment and Preparation of TiO$_2$-TP Composite Coating

2-1. Preparation of TiO$_2$-TP Composite

As an extension of the study, in which leaf extract is used directly for inhibition, the optimized composition was further used to synthesize a composite with TiO$_2$, the most important material used by paint industry for whiteness and opacity. TiO$_2$ powder (Merck, assay>99.9%, CAS No: 1317-80-2) was purchased. 50 mL, 500 ppm of ethanolic TP extract was taken. To which 0.1 g of TiO$_2$ was added and then ultra-sonicated. Then the solution was kept for two days at room temperature for aging. Thereafter, excess solvent was removed by rota-vapor and then dried in an oven at 60 °C [23-25].

2-2. Fabrication of TiO$_2$-TP Composite Coated Mild Steel

Mild steel coupons of composition Fe-92.56%, CO-0.125%, Mn-0.0641%, Si-0.94%, P-0.019%, S-0.164%, Cr-0.012%, Mo-0.019%, were used. Steel strips with the dimension of $3 \times 2.4 \times 0.1$ cm^3 were polished to mirror finish, degreased with trichloroethylene, and then washed with distilled water. Thus pre-treated steel coupons were used to coat the bio-composite. In the proposed coating procedure, PVC (granules, Auto grade) was used as an adhesive. 0.002 g of TiO$_2$-TP composite was dispersed well in a solution of 0.5 g PVC in 60 mL THF. Immediately the mix was brush coated on the pre-treated mild steel surface and kept aside to dry for 12 h [25]. To elucidate the effect of leaf extract loading, a coating was also pre-

pared with TiO$_2$-PVC mix without extract by the same procedure. Schematic representation of the entire synthesis and fabrication strategy are illustrated in Fig. 1.

3. Characterization Techniques

3-1. Characterization of the Ethanolic Extract

The chemical constituents in the ethanolic extract of TP leaf extract are well established [17-20]. Preliminary confirmation of the composition of the extract was done by qualitative analyses. We analyzed alkaloids, carbohydrates, glycosides, phytosterols, terpenoids, saponins, tannins, protein, amino acids, flavonoids, terpenoids, and phenols. The details of the analyses are given in the supplementary information. FTIR analysis was carried out (FTIR Perkin-Elmer spectrophotometer) to identify the active functional groups present in the TP leaf extract. For this, 10 mg of the dried extract was pelletized with 100 mg of KBr and then loaded into an FTIR spectroscope and scanned over the range of 400-4,000 cm^{-1}.

3-2. Characterization of TiO$_2$-TP-PVC/Mild Steel (TiO$_2$-TP-PVC/CS)

Water contact angle (θ) expresses the surface affinity for water. If for a surface $\theta<90°$, implies the hydrophilic nature of the surface. If $\theta>90°$, the surface is hydrophobic. Surface attains a superhydrophobic behavior when $\theta \geq 150°$ [25]. In the present work, water contact angle of TiO$_2$-TP-PVC/CS and TiO$_2$-PVC/CS was measured (Kraus DSA 30 drop shape analyzer at R.T) in order to reveal the surface affinity for water molecules. The surface topography of TiO$_2$-TP-PVC/CS and TiO$_2$-PVC/CS was recorded by OSP imaging. The topographical images were recorded before and after five days immersion in 1 M HCl. The imaging was carried out in M370 scanning electrochemical work station 4.50.5147, 64 bit operating system, uni scan instrument Ltd.UK.

3-3. Characterizations Used for the Evaluation of Anti-corrosive Performance

3-3-1. Weight Loss Measurement- Adsorption isotherm-Effect of Temperature on Corrosion Rate

The mild steel coupons were immersed in 100 mL of the pre-

pared leaf extract solutions for 8 h. After the immersion period, the corrosion product was cleaned with Clark's solution composed of 93% HCl, 5% SnCl$_2$ and 2% Sb$_2$O$_3$. The weight of the specimen before and after immersion in inhibitor solution was determined. Specimen immersed in 100 mL 1 M HCl (without inhibitor) was also evaluated for comparison. Corrosion rate was calculated assuming uniform corrosion over the entire surface of the steel coupon. The inhibition efficiency, corrosion rate and surface coverage were calculated using the following expressions [9];

$$IE = \left[1 - \frac{W_2}{W_1} \right] \times 100\%$$

$$\text{Surface coverage } (\theta) = \left[1 - \frac{W_2}{W_1} \right]$$

where, W$_1$=weight loss in the absence of inhibitor; W$_2$=weight loss in the presence of inhibitor;

$$\text{Corrosion Rate} = \frac{W \times 87.6}{DAT}$$

where W is the weight loss (g); D, density of the steel coupon (g/cm^3); A, area of the coupon (cm^2) and T, the time of immersion (h).

The weight loss data was further used to identify the adsorption isotherm best suited to explain the adsorption mechanism of corrosion inhibition.

3-3-2. Electrochemical Characterization

Potentiodynamic polarization was carried out using a three electrode system - mild steel specimen with an exposed area of 1 cm^2 as the working electrode, Ag/AgCl was used as the reference electrode and a platinum wire was used as the counter electrode. Polarization curves were recorded by scanning potential from -0.7 V to $+0.7$ V at a scan rate of 0.01 V/s. E$_{corr}$, I$_{corr}$, β_a, β_c etc. were computed from the polarization curves. Inhibition efficiency was calculated using the following expression [9,24];

$$IE = \frac{I_{corr} - I'_{corr}}{I_{corr}} \times 100$$

where I$_{corr}$ and I'$_{corr}$ are the corrosion current in solution without and with inhibitor, respectively.

Electrochemical impedance spectroscopy (EIS) was used to measure the impedance of the system. EIS measures the resistance and capacitance properties of the electrode via application of a sinusoidal AC excitation signal of 5 mV at OCP (open circuit potential). Nyquist plots were recorded over the frequency range 10 mHz to 100 kHz at its open circuit potential. Scan rate is 1 mV/s. The following expression is used to evaluate the inhibition efficiency of the system:

$$IE = \frac{C_{dl} - C'_{dl}}{C_{dl}}$$

where C'$_{dl}$ and C$_{dl}$ are the charge transfer resistances of mild steel in solution with and without inhibitor. The experimental setup for impedance analysis is identical to that used in potentiodynamic polarization study. R$_{ct}$, C$_{dl}$, R$_s$, R$_f$ etc. were derived from the Nyquist plot. Bode plots were also recorded with log frequency vs. log Z. All the electrochemical analyses were performed using electrochemical work station, Biologic Science Instrument, SP 200 (using EC-Lab software, version 10.38).

3-4. OCP Measurement (Open Circuit Potential)

Long-term corrosion protection capability of TP leaf extract was confirmed using OCP measurement. The open circuit potential (corrosion potential) of the specimen immersed in HCl solution containing different concentration of the inhibitor (100 ppm, 200 ppm, 300 ppm and 500 ppm) was measured using Abbe digital multimeter using Ag/AgCl as the reference electrode, for 30 days. OCP of TiO$_2$-TP-PVC/CS and TiO$_2$-PVC/CS was also measured in HCl, HCl (80 °C) and rainwater medium.

3-5. Characterization Used for the Confirmation of Mechanism of Corrosion Inhibition

The mild steel coupons were immersed in inhibitor solution for three days. Thereafter it was recovered from the solution, washed (mildly) with distilled water, and dried. The scale developed over the coupons was analyzed using an energy dispersive spectrometer attached to SEM (scanning electron microscopy) instrument (JEOL JSM-840A; JOEL Model JED- 230). UV-Visible spectra of 500 ppm TP leaf extract before and after immersion (3 days) were recorded to confirm the adsorptive behavior of chemical constituents in the inhibitor solution on the metal surface (Schimadzu UV 2450 spectrometer over the wavelength range 200-800 nm).

RESULTS AND DISCUSSION

1. Characterization of the Ethanolic Extract of Thespesia Populnea (TP)

1-1. Chemical Composition of TP Leaves Extract

The composition of ethanolic extract of TP leaves was recognized in several phytochemical studies [17,18]. Table 1 shows the

Table 1. The major chemical constituents present in ethanolic TP leaf extract derived from HPLC study

| Name of the compound	Molecular weight	Retention time (min)
9, 12-Octadecadienoic acid (Z,Z)- (Synonyms: Linoleic acid)	280	19.72
n-Hexadecanoic acid	256	16.82
2,6,10,14,18,22-Tetracosahexaene, 2,6,10,15,19,23- hexamethyl-. [all-E}- (Synonyms: *trans*-Squalene)	410	31.04
Phytol	296	19.10
3,7,11,15-Tetramethyl-2-hexadecen-l-ol	296	14.87
1,2-Benzenedicarboxylic acid, diisooctyl ester	390	25.9
Ethyl oleate	310	20.71
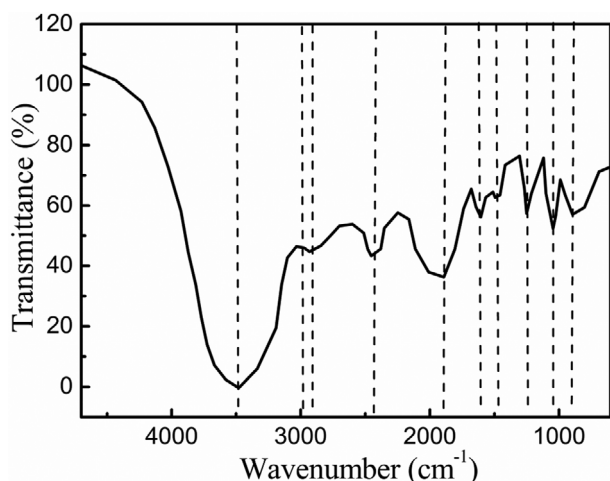
Fig. 2. IR spectrum of TP leaf extract.

major chemical constituents present in ethanolic TP leaf extract derived from HPLC study [19]. Qualitative analyses were also performed for detecting the presence of alkaloids, carbohydrates, glycosides, phytosterols, terpenoids, saponins, tannins, protein, amino acids, flavonoids, terpenoids, and phenols. The results of preliminary analysis are given in Table S1. Graph of HPLC analysis is given as Fig. S1.

1-2. IR Analysis of the Leaves Extract

IR spectroscopy was further used to confirm the results obtained for qualitative analyses. The FTIR spectrum of the ethanolic TP extract is shown in Fig. 2. The broad vibrational band at 3,485.12 cm^{-1} represents O-H stretching vibration in alcohols and phenols. The less intense band obtained at 2,916.75 cm^{-1} resulted from the stretching vibrations of aliphatic C-H, CH$_2$, and CH$_3$ groups. O-H stretching vibrations of carboxylic acid made the band present at 2,430.58 cm^{-1}. O-H bending vibrations in aromatic compounds are identified by the band found at 1,980 cm^{-1} [5]. The peak at 1,240 cm^{-1} implied C-O stretching in phenols. The band observed at 1,616 cm^{-1} arose from the C=C stretching vibrations. Bands at 1,490 cm^{-1} and 1,350 cm^{-1} may have arisen from carboxylic acid's coupled C-O and O-H stretching vibration [9]. Bending vibrations of the O-H group of carboxylic acid/alcoholic C-O group are identified from the peak positioned at 1,050 cm^{-1}. The band at 937 cm^{-1} and 887 cm^{-1} resulted from the alkenic C-H vibrations [20,26]. Therefore, the prepared TP leaf extract is rich in carbohydrates, acids, terpenes, and phenolic compounds. These compounds produced a positive result in the performed qualitative chemical analysis also.

Hence the constituent components recorded in Table 1 agree with the FTIR results [20,26].

2. Anti-corrosive Activity of TP Leaves Extract

2-1. Evaluation by Weight Loss Method

2-2-1. Weight Loss Method- Adsorption Isotherm

The inhibition efficiency of prepared concentrations of TP leaf extract towards mild steel corrosion in 1M HCl medium was investigated for 8 h. The result recorded in Table 2 indicates that the rate of corrosion decreases with increase in concentration of inhibitor solution. 500 ppm solution of TP leaf extract exhibited an inhibition efficiency of 98.24% with a surface coverage of 0.9824. 300 ppm solution can also produce a significant inhibition efficiency of 96.67% [9].

It is well known that the inhibition effect of a green inhibitor is based on the adsorption of the organic constituents at the metal/solution interfaces; therefore, it is imperative to understand the adsorption behavior of the inhibitor in order to reveal its inhibition mechanism. The adsorption isotherm can provide vital information regarding the interaction between the inhibitor and the metal surface. Adsorption of the inhibitor molecules mainly depends on the metal surface's charge and nature, electronic characteristics of the metal surface, temperature, adsorption of the solvent, ionic species, and the electrochemical potential at the solution interface. The most frequently used adsorption isotherms are Langmuir, Temkin, Friedmann and Freundlich. To obtain the adsorption isotherm, the degree of surface coverage (θ) was calculated for various concentrations of the TP extract from the weight loss data. Langmuir adsorption isotherm was tested to fit with the experimental data. Langmuir adsorption isotherm is represented by the equation [27]:

$$\frac{C}{\theta} = \frac{1}{K_{ads}} + C_{inh}$$

where, K$_{ads}$ is the adsorption equilibrium constant, θ is the degree of surface coverage and C$_{inh}$ is molar concentration of the inhibitor used. A straight line graph was obtained on plotting C$_{inh}$/θ vs. C$_{inh}$ and the regression coefficient was almost equal to unity (Fig. 3). Thus, the Langmuir adsorption isotherm was the best to describe the adsorption behavior of the components of the TP extract on the metal surface. The Langmuir assumes that the metal surface is covered by a monolayer of inhibitor molecules and there is no interaction between adjacently adsorbed molecules. The parameters computed from the adsorption isotherm are given in Table 3. From the intercept of the straight line in Fig. 3, the values of K$_{ads}$ and free energy change during the reaction were calculated. K$_{ads}$ is obtained from the intercept of the graph and the free energy change

Table 2. Results of weight loss study with TP leaf extract in different concentration

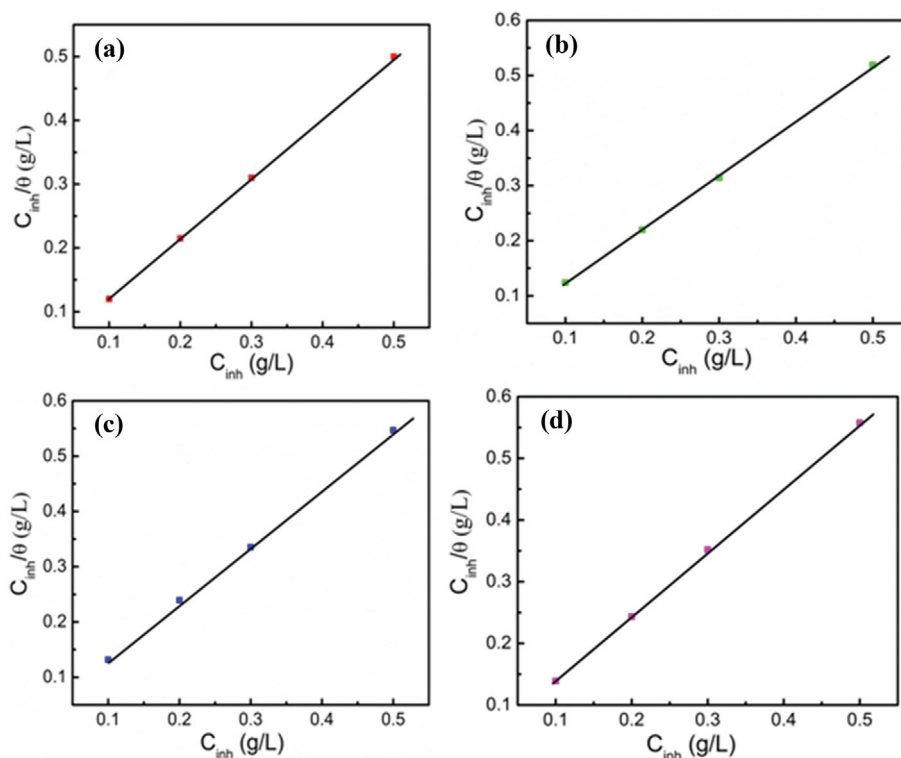| Inhibitor system	Weight loss (g)	Inhibition efficiency (%)	Surface coverage (θ)	Corrosion rate (g cm^{-2} h^{-1})
Blank	0.0931	-	-	2×10^{-4}
100 ppm	0.0176	81.10	0.8110	3.7×10^{-5}
200 ppm	0.0067	92.80	0.9280	1.4×10^{-5}
300 ppm	0.0031	96.67	0.9667	6.7×10^{-6}
500 ppm	0.0016	98.24	0.9824	3.4×10^{-6}

Fig. 3. C$_{inh}$ vs. C$_{inh}$/θ plot obtained at (a) 298 K (b) 308 K (c) 318 K (d) 328 K.

Table 3. Parameters obtained from Langmuir adsorption isotherm

Temperature (°C)	K$_{ads}$ (g^{-1}L)	Slope	R^2	ΔG (kJ/mol)	ΔH$_{ads}$ (kJ)
298	3.74	1.132	0.9989	−13.18	−34.39
308	2.86	1.089	0.9976	−12.95	
318	1.76	1.058	0.9963	−12.08	
328	1.06	1.029	0.9925	−11.08	

during the adsorption process is calculated using the following equation [9,27];

$$\Delta G = -2.303RT\log 55.5K_{ads}$$

where, ΔG represents the Gibb's free energy of adsorption; T, the temperature; K$_{ads}$ is the equilibrium constant of adsorption and 55.5 is the molar concentration of water in inhibitor solution. The negative free energy value (−13.18 kJ/mol) obtained for the adsorption process ensured spontaneous adsorption of inhibitor molecules on the mild steel surface. ΔG values of −20 kJ/mol or less negative are associated with physisorption, which may be caused by the electrostatic interaction between components of the inhibitor solution and charged metallic surface. For adsorption with ΔG more negative than −40 kJ/mol implies the possibility of chemical adsorption. Thus, here the adsorption of TP extract on the surface of mild steel is said to follow physical adsorption mechanism. It can be seen that as the temperature increases K$_{ads}$ decreases, which signifies that the strength of adsorption decreases with increase in temperature. This temperature dependence also confirmed the physical adsorption mechanism of corrosion inhibition. Also,

the negative value for ΔG decreases with increase in temperature, attributed to the decreasing trend of spontaneous adsorption. The enthalpy change associated with the adsorption process is evaluated using integrated form of the van't Hoff equation [9]:

$$\ln K_{ads} = \frac{-\Delta H_{ads}}{RT} + \frac{\Delta S_{ads}}{R} + \ln\frac{1}{55.5}$$

A graph plotted between 1,000/T vs. logK$_{ads}$ is illustrated in Fig. S2. The enthalpy change associated with the adsorption of TP leaf extract on mild steel surface was −34.39 kJ and is calculated from the slope of Fig. S2. The negative value for the enthalpy change accounted for the exothermic nature of the adsorption process. The result could also explain the temperature dependence on adsorption behavior and hence on the inhibition efficiency [28,29].

2-2-2. Effect of Temperature on Corrosion Rate

Effect of temperature on corrosion rate and inhibition efficiency was evaluated for the temperature range 298 K-328 K. Inhibition efficiency and corrosion rate of various concentrations of TP leaf extract evaluated at 298 K, 308 K, 318 K, 328 K are given in Table 2, Table S2, Table S3 and Table S4, respectively. Inhibition efficiency of TP leaf extract against mild steel corrosion in 1 M HCl medium decreases with increase in temperature. This was focused on the fact that components of TP leaf extract offer effective inhibition by physical adsorption. Temperature dependence on corrosion rate can be expressed by the Arrhenius relation:

$$CR = Ae^{\frac{-E_a}{RT}}$$

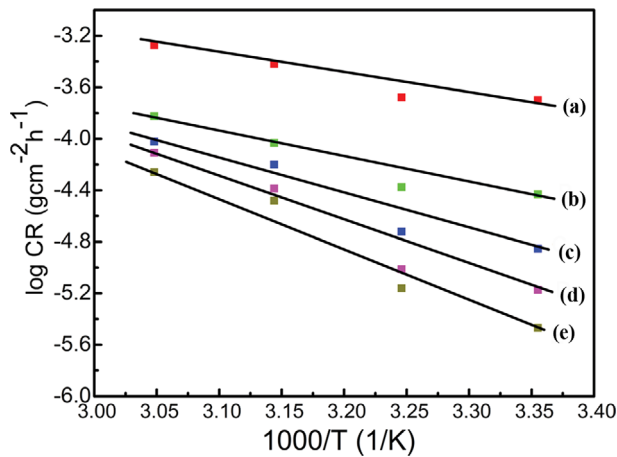where CR, the corrosion rate constant; E$_a$, the activation energy;

Fig. 4. Arrhenius plot of TP leaf extract obtained over the temperature range 298 K-328 K at concentrations (a) 0 ppm (b) 100 ppm (c) 200 ppm (d) 300 ppm (e) 500 ppm.
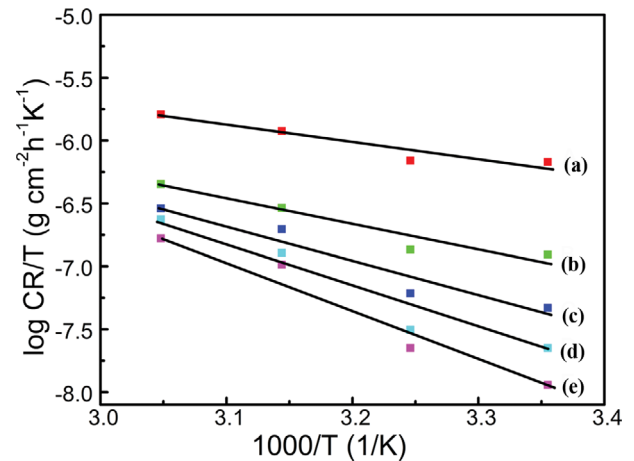

Fig. 5. Variation of log(CR/T) with 1/T over the temperature range 298 K-328 K for TP leaf extract at (a) 0 ppm (b) 100 ppm (c) 200 ppm (d) 300 ppm (e) 500 ppm.

Table 4. Thermodynamic parameters obtained for TP leaf extract/ CS system at different extract concentrations

Concentration (ppm)	E_a (kJ/mol)	ΔH_a (kJ/mol)	ΔS (JK^{-1}mol^{-1})
0 ppm	40.78	−38.29	−104.51
100 ppm	44.43	−41.65	−68.72
200 ppm	54.23	−51.76	−51.43
300 ppm	67.91	−65.43	−32.76
500 ppm	70.68	−68.21	−21.42

A, Arrhenius constant; R, universal gas constant; T, the temperature. The values of E_a for mild steel in HCl solution containing various concentrations of TP leaf extract and without leaf extract at different temperatures were computed from the linear regression coefficient of the Arrhenius plot given in Fig. 4. It can be seen that E_a value increases with increase in extract's concentration (Table 4), Further confirming the physical adsorption of TP leaf extract on mild steel surface. The increase in E_a value indicates the difficulty in dissolution of metal surface in solutions of high inhibitor concentration. As the inhibitor concentration increases, the enhanced physical adsorption hinders the interaction between corrosive electrolyte and metal surface.

The enthalpy and entropy of activation associated with the corrosion process (ΔH_a and ΔS_a) can be computed from the transition state theory using the following relation:

$$CR = \frac{RT}{Nh} e^{\Delta S_a/R} e^{-\Delta H_a/RT}$$

where N, Avogadro's number; h, Planck's constant. Fig. 5 shows the variation of log(CR/T) vs. 1/T. Straight lines are obtained for metal in blank as well as all inhibitor solutions, with slope $\frac{-\Delta H_a}{2.303R}$ and intercept $\log\frac{R}{Nh} + \frac{\Delta S_a}{2.303R}$. ΔH_a and ΔS_a values were calculated for solutions with and without inhibitors and tabulated in Table 4. Positive values for ΔH_a suggested that activated complex formation is an endothermic process and therefore the metal dissolution follows slow kinetics. As predicted by the transition state theory the variation in ΔH_a and E_a was related as $E_a = \Delta H_a + RT$. Entropy of activation increases during the complex formation indicated that the extent of disorder increases during the activation process. Degree of disorder increases with increase in concentration of inhibitor solution [9,27,30,31].

2-2. Tafel Polarization

Potentiodynamic polarization was further carried out to retrieve the inhibitive parameters such as I_{corr}, E_{corr}, β_a, β_c and R_p of the proposed system [32,33]. The inhibition efficiency of organic constituents in the green extract depends on the electron density of its adsorbate functional groups. That is, the higher the electron density of the inhibitor, the higher will be the inhibition efficiency. Table 5 records the corrosion characteristics obtained from the study at

Table 5. Tafel parameters derived from polarization study

Inhibitor system	E_{corr} (V)	I_{corr} (μA cm^{-2})	R_p (Ω cm^2)	β_a (V/dec)	β_c (V/dec)	θ	IE (%)
Blank	−0.532	188.1	654	0.202	0.265	-	-
100 ppm	−0.484	39.4	5,384	0.187	0.246	0.790	79.5
200 ppm	−0.468	18.5	11,530	0.168	0.223	0.904	90.4
300 ppm	−0.417	8.6	21,729	0.157	0.208	0.953	95.3
500 ppm	−0.340	5.5	35,824	0.142	0.196	0.97	97.1

Fig. 6. Tafel plots derived for TP/CS system at different extract concentrations.

Fig. 7. Nyquist plots derived for TP/CS system at different extract concentrations.
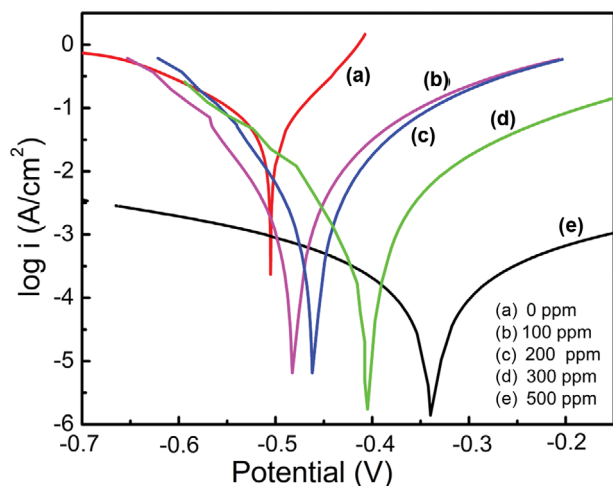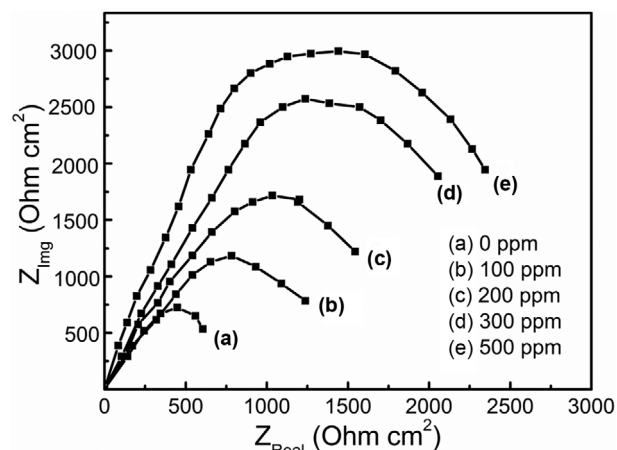

Fig. 8. Bode plots of TP/CS system at different extract concentrations.

298 K. There was a significant reduction in I$_{corr}$ value with increase in inhibitor concentration and the lowest I$_{corr}$ value (5.5 µA cm^2) was observed with 500 ppm solution, which might be due to the formation of a stable passive barrier layer by the components of TP leaf extract on the steel surface. The Tafel lines corresponding to both cathodic and anodic polarization of inhibitor system were found to have shifted to more positive and negative potential relative to the plots of blank solution (Fig. 6). This observation illustrates that the extract could suppress both anodic and cathodic dissolution and hence can be called as a mixed type inhibitor. But as the concentration of the inhibitor increased, E$_{corr}$ slightly shifted towards positive region so that the TP leaf extract has inhibitive action a little more on anodic dissolution rather than cathodic hydrogen evolution. The values of β_a and β_c were found almost steady bringing out the point that TP leaf extract resist anodic metal dissolution and cathodic hydrogen evolution without altering their actual mechanism. R$_p$, value was also found maximum for 500 ppm of the leaf extract [34-36].

2-3. EIS-Bode Plot

The resistive and capacitive behavior of interaction at the metal/electrolyte interface could be successfully explained by electrochemical impedance spectroscopy. When mild steel is immersed in inhibitor solution, a double layer of opposite charge will be formed at the interface. EIS enables us to calculate the double-layer capacitance (C$_{dl}$), surface resistance towards electron transfer, solution resistance towards electron transfer, and various impedance terms that arise from the migration of ions towards or away from the electrolyte [37-40]. The circuit diagram used to explain the electrochemical reaction at the mild steel surface-TP leaf extract interface is given in Fig. S3. The diagram contains two resistive and capacitive components. The Nyquist plots and Bode plots obtained for the systems are given in Fig. 7 and Fig. 8, respectively. The single semicircle in the Nyquist plot indicates that the reaction is characterized by a single time constant and, therefore, a single electron transfer reaction. The higher R$_{ct}$ value obtained with 500 ppm solution refers to the higher surface resistance towards electron transfer reaction. The 500 ppm solution has offered the maximum resistance towards
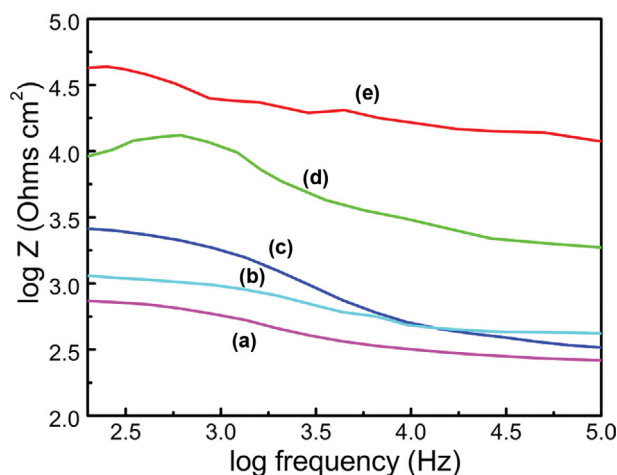
Table 6. Parameters derived from EIS analysis

Inhibitor system	R$_{ct}$ (Ω cm^{-2})	R$_s$ (Ω cm^{-2})	C$_{dl}$ (µF cm^2)	R$_f$	IE (%)
Blank	812	1.8	284.65	1.12	-
100 ppm	1,645	2.2	54.72	0.21	80.7
200 ppm	2,314	2.5	26.35	0.104	90.7
300 ppm	2,684	2.7	13.57	0.051	95.23
500 ppm	2,915	3.1	8.34	0.032	97.12

the charge transfer process. As the concentration of the inhibitor solution increases, a decreasing trend is observed in the C$_{dl}$ value. The decrease in C$_{dl}$ value confirms the increase in thickness associated with the double layer formed. This has further implied the formation of a stable, protective layer over the metal surface with an increase in inhibitor concentration. The formation of a uniform and smooth coating on the metal surface due to the adsorption of phytochemical constituents at a higher concentration of inhibitor solution is explored by its low surface roughness value [41-45]. The
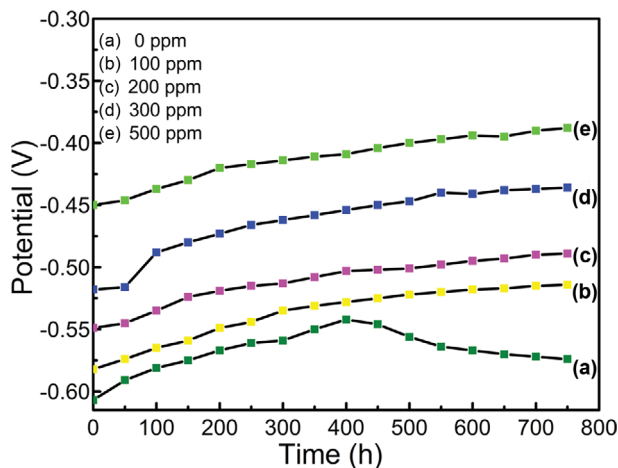
Fig. 9. OCP decay obtained for mild steel observed for 30 days.

parameters derived from EIS analyses are in Table 6.

2-4. Long-term Activity by OCP Measurement

Long-term protective efficiency of TP leaf extract for mild steel is explored by measuring its open circuit potential for a period of 30 days. Fig. 9 illustrated the change in open circuit potential of the mild steel with time, in inhibitor solution of varying concentrations.
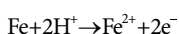
The values of OCP taken as the average of last three readings were found to be −0.390 V, −0.435 V, −0.490 V, −0.514 V, −0.558 V, respectively, for 500 ppm, 300 ppm, 200 ppm, 100 ppm and 0 ppm inhibitor solution. The initial decrease in potential observed implied dissolution of the air formed metal oxide layer on the steel coupon. Later, within 3-4 days it can be seen that system attained a steady potential. The observation indicated the formation of a stable barrier layer over the metal surface by the adsorption of phytochemical constituents. That is, the active organic components present in the inhibitor solution diffuse to the metal surface and get adsorbed on it. The initial changes in potential refer to the process of formation of the layer, and the complete coverage of metal surface by the passive layer is ensured by the stable potential acquired by the system. As the concentration of inhibitor solution increases, corrosion potential shifts towards positive region attributed to the cathodic nature of passive film formed by the extract solution at higher concentration [46-49].

3. Mechanism of Corrosion Inhibition

The corrosion process of mild steel in acidic medium can be written as [9,27],

$$Fe \rightarrow Fe^{2+} + 2e^- \text{ (anodic process)}$$

$$2H^+ + 2e^- \rightarrow H_2 \uparrow \text{ (cathodic process)}$$
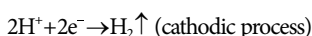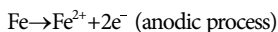
The overall corrosion mechanism is given as,

$$Fe + 2H^+ \rightarrow Fe^{2+} + 2e^-$$

The primary constituents present in TP leaf extracts were identified by IR and HPLC. Carbohydrates, acids, terpenes and phenolic compounds were identified as the major constituents in TP leaf extract (Table 1). The hydroxyl and carbonyl groups present in the

extract possess anti-oxidant property. In HCl medium the unstable $Fe(OH)_2/Fe(OH)_3$ begins to form oxy-hydroxide layer. Although this passive layer can act as a barrier between metal and electrolyte initially, continuous Cl^- attack will rupture the layer and initiate metal dissolution and end up in rust formation.

$$Fe(OH)_2/Fe(OH)_3 \rightarrow FeO(OH)_2 \rightarrow Fe_2O_3/Fe_3O_4$$

The stability of the oxy-hydroxide layer is enhanced by the adsorption of inhibitor molecules at the metal/solution interface. The adsorption occurs by the replacement of solvent molecules from the metal surface or from the vicinity of metal/solution interface by ions of inhibitor molecules [21]. The adsorption can happen either through electron-rich hetero atoms present in fatty acids, phenolic compounds etc. or through pi-electrons present in terpenes. The electron-rich hetero atoms replace solvent molecules in the metal surface and get adsorbed on the metal. The pi-electrons interact with the charged metal ions [9,12,24,26]. There does not occur transfer or sharing of electrons. The association between Fe^{2+} and TP in the complex is not by a coordinate covalent bond, evidenced by the less negative ΔG value of −13.18 kJ/mol [26].

$$FeO(OH) + TP \text{ leaf extract} \rightarrow Fe^{2+} - TP$$
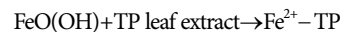
$Fe^{2+}-TP$ complex thus formed is able to withstand at Cl^- attack. The formation of the passive layer is evidenced from OCP values, polarization study and weight loss measurements, as discussed in the sections 3.2.1, 3.2.2 and 3.2.4, respectively. In addition, direct evidence for the formation of passive layer by the components of TP leaf extract is obtained from EDS and UV-Vis spectral data. EDS of the passive film formed over the metal surface is given in Fig. 10. The presence of carbon and oxygen confirmed that it is formed by the adsorption of phytochemicals on the metal surface. The spectrum reiterated that the protective layer is $Fe^{2+}-TP$ complex.

UV-Visible spectrum of 500 ppm TP leaf extract obtained before and after immersion (3 days) of mild steel coupon is shown in Fig. 11. UV-Vis spectrum of 500 ppm of TP leaf extract displayed an
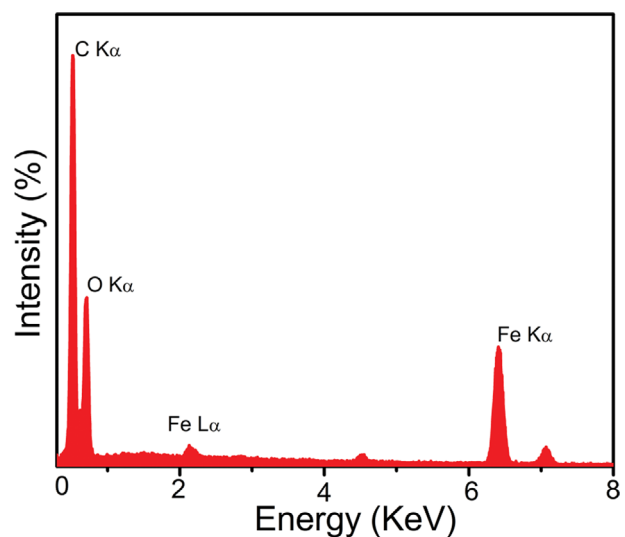

Fig. 10. EDS of the Passive film formed over the metal surface in presence of TP extract.
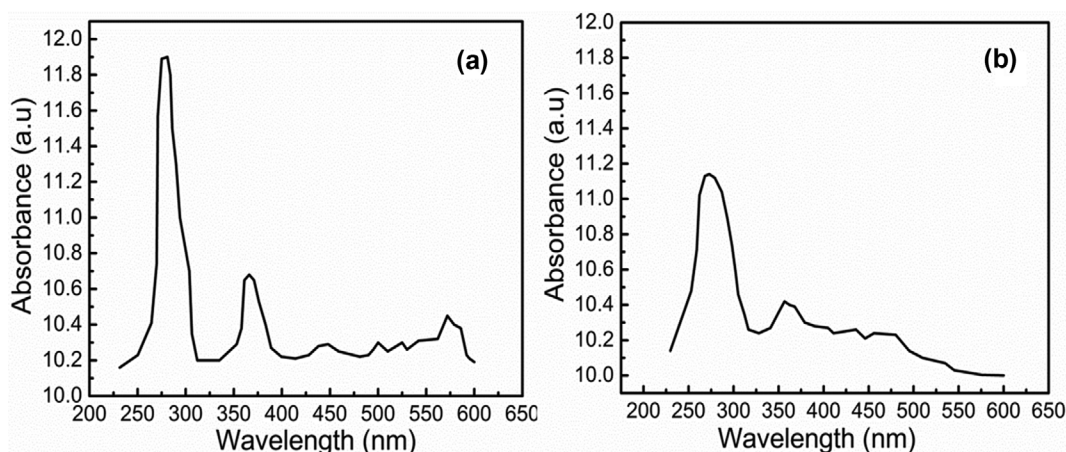
Fig. 11. UV-Visible spectrum of 500 ppm TP leaf extract obtained (a) Before immersion (b) After immersion.

intense peak at 280 nm, resulted from the n-π*, π-π* transitions in the components. Whereas, the spectrum obtained with the same solution after immersion study contains the most intense peak at 270 nm. Also, the intensity of the peak is considerably reduced compared to the pure extract [21]. The blue shift, as well as intensity reduction, throws light on the Fe^{2+}–TP complex formation [9].

The migration of phytochemical constituents in the leaf extract on to the metal surface and its complex formation with Fe^{2+} ions were substantiated by the results obtained from EDS & UV-Visible studies.

4. TP Leaves Extract: A Promising Green Inhibitor for Mild Steel

A comparative study on efficiency of TP leaf extract with already reported green inhibitor systems is recorded in Table 7 in order to expose the significance of the study. The ease of availability of the plant material, simplicity of extract production, efficiency of inhibition and long term protective activity have made TP leaf extract a versatile inhibitor for mild steel corrosion in acidic environment. On analysis it is found that the investigated TP leaf extract pos-

sessed the least I_{corr} value among the recorded green inhibitor systems. The performance of the leaf extract is superior to other systems in terms of R_{ct} and C_{dl} values. The inhibition efficiency calculated from weight loss, Tafel and EIS analysis for all the systems confirmed a superior/comparable inhibition performance of the leaf extract.

5. Proposal for Application of TP Leaves Extract in Paint Industry

To divulge the applicability of TP leaf extract in paint, here composited the plant extract with TiO₂. Painting is one of the most established corrosion protection strategies, and TiO₂ is the primary pigment used in the paint industry, imparting white color and opacity. It is primarily responsible for protecting white and light-colored paints from weathering. Proper modification of the TiO₂ pigment could make paints resistant to weathering and other accelerated environments, enabling them for use for industrial applications. Here a TP-TiO₂ composite was fabricated and brush coated onto a pre-treated mild steel surface as discussed in section 2.2. The following sections discuss the characteristics of the coating and its anti-corrosive performance for mild steel in 1 M HCl medium,

Table 7. Performance comparison of TP leaf extract with already established green inhibitor systems

Inhibitor system	Medium	Optimum concentration	I_{corr}	IE (WL, PP, EIS) (%)	R_{ct} (Ω cm²)	Ref.
Pongamia pinnata leaf extract	1 N H₂SO₄	100 ppm	0.11 mA/cm²	94.64,74.97, 70	102	[4]
Lagerstroemia speciosa leaf extract	1 M HCl	500 ppm	2.86×10^{-4} A/cm²	94.41,76.32, -	-	[7]
Sesbania grandiflora leaf extract	1 M HCl	10,000 ppm	0.134×10^{-6} A/cm²	98.01, 97.2, 94.4	910	[9]
Pineapple stem extract	1 M HCl	1,000 ppm	4.83×10^{-5} A/cm²	97.6, 95.4, 96.69	443.1	[10]
Radish leaf extract	0.5 M H₂SO₄	300 mg/L	0.11±0.01 mA/cm²	93, 94.11, 92.19	118.9±1.9	[12]
Loquat (Eriobotrya japonica Lindl.) leaves Extract	0.5 M H₂SO₄	100 ppm	0.021 mA/cm²	81.1, 74.9, 67.0	596	[27]
Ginkgo leaves extract	1 M HCl	200 mg/L	34.7 µA/cm²	-, 90, 89.9	643	[30]
Extract of Citrus sinensis	0.5 M H₂SO₄	500 mg/L	0.00005816 A/cm²	96.62, 93.47, 94.73	477.84	[40]
Laurus nobilis extract	1 M HCl	400 ppm	0.29±0.02 mA/cm²	-, 92%, -	479.7±31.2	[41]
Eucalyptus leaf extract	H₂SO₄	0.4 g/L	0.46 mA/cm²	-, -, 91	107.9	[51]
	H₃PO₄	0.3 g/L	0.34 mA/cm²	-, -, 78	77.3	[51]
Thespesia Populnea leaves extract	1 M HCl	500 ppm	5.5 µA/cm²	98.24, 97.1, 97.12	2915	Present work

1 M HCl at 80 °C, and rainwater medium.

5-1. Contact Angle Measurement of TiO$_2$-TP-PVC/CS

Measurement of contact angle enables the prediction of hydrophilic/hydrophobic nature of the fabricated surface [50]. The hydrophilic to ultra-hydrophobic transition of composite coated mild steel surface can be seen in Fig. 12. The surface coated with TiO$_2$ (TiO$_2$-PVC/CS) demonstrated a water contact angle (WCA) of 117.7°, whereas TiO$_2$ composited with TP leaf extract coated steel surface
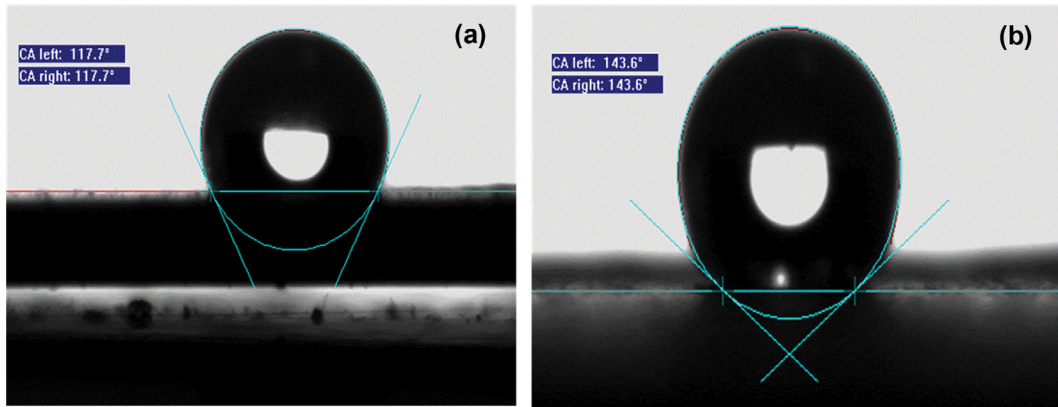

Fig. 12. Contact angle images obtained for (a) TiO$_2$-PVC/CS (b) TiO$_2$-TP-PVC/CS.

Table 8. Surface roughness data obtained on OSP imaging

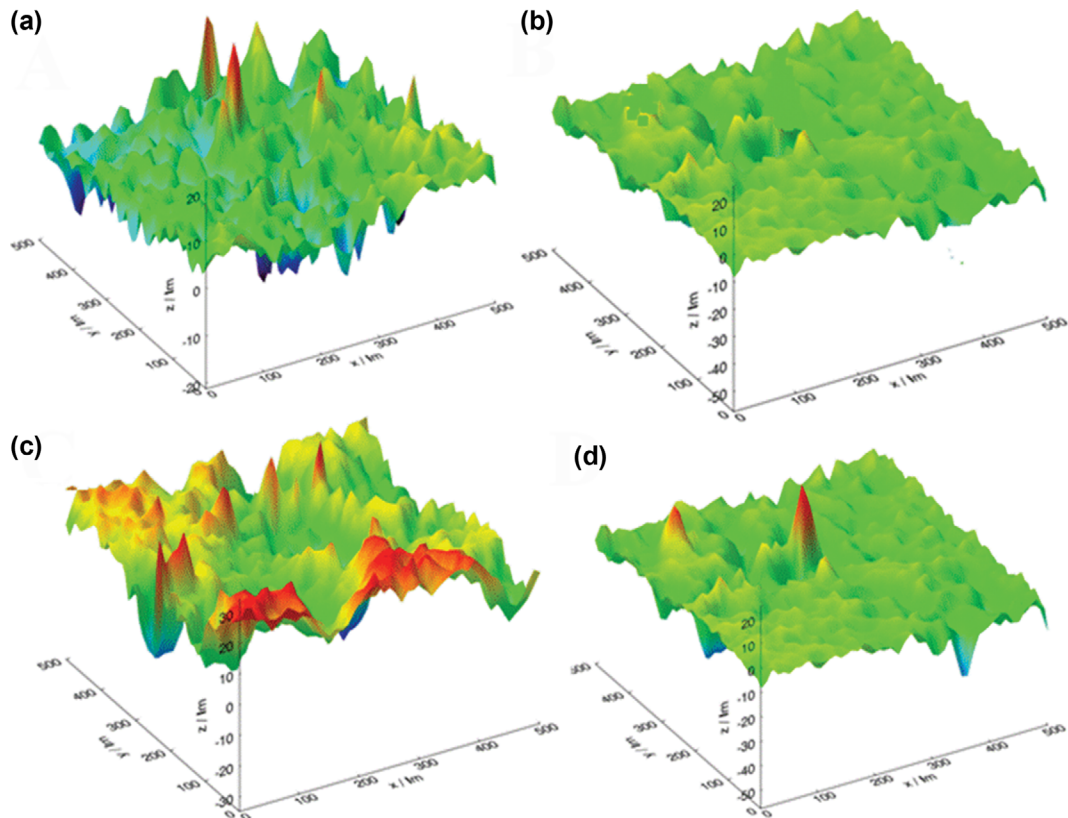| Coatings	S$_a$ (μm)	S$_q$ (μm)	S$_p$ (μm)	S$_v$ (μm)	S$_{sk}$ (μm)	S$_{ku}$ (μm)
TiO$_2$-PVC/CS	4.23	5.46	36.1	−39.6	0.75	2.75
TiO$_2$-TP-PVC/CS	3.24	4.72	23.2	−21.8	0.42	2.41

Fig. 13. Profilometric images obtained for (a) TiO$_2$-PVC/CS, before immersion (b) TiO$_2$-TP-PVC/CS, before immersion (c) TiO$_2$-PVC/CS, after five days immersion in 1 M HCl (d) TiO$_2$-TP-PVC/CS, after five days immersion in 1 M HCl.

(TiO$_2$-TP-PVC/CS) exhibited a considerably higher value for WCA (143.6°). The extreme water repellency could be recommended as a sign of corrosion resistant behavior [25,27,50].

5-2. Surface Study: OSP (Optical Surface Profilometry) Imaging

Optical surface profilometry was performed to investigate the surface topography of composited extract coated metal surface. The ups and downs in the images represent the roughness intensity in the coating. The various roughness parameters, S$_a$, S$_q$, S$_p$, S$_v$, S$_{ku}$, S$_{sk}$ etc. [38], of the coatings are in Table 8. Average roughness (S$_a$) indicates the arithmetic mean of deviation of surface height with respect to the mean plane. The standard deviation of surface height is represented by S$_q$. The height of the largest intense peak provides the value of S$_p$. The deepest valley depth is indicated by S$_v$. Symmetry of the surface with respect to the mean plane is shown by S$_{sk}$. S$_{ku}$ reveals the surface kurtosis value.

The low S$_a$ value of composite coated surface implies its corrosion-resistant behavior. S$_q$ value is observed as low, attributed to the minimum surface roughness, which further implies the protective nature of the coating. The absence of peaks and valleys on the composite coated surface is divulged by the low value of surface kurtosis, which is less than 3. The surface smoothness is evident from the nearly zero value obtained for the surface skewness term (S$_{sk}$). The maximum peak height (S$_p$) and maximum valley depth (S$_v$) are also embedded in the table. OSP imaging of coating, after immersion in 1 M HCl, was also obtained. It can be seen that surface roughness of TiO$_2$-PVC/CS increases after five days of immersion in 1 M HCl medium. Surprisingly, TiO$_2$-TP-PVC/CS was not affected significantly, except some minute alternations [40]. The composited extract coated surface is remarkably resistant to corrosion in acidic environment, which is obviously seen in Fig. 13.
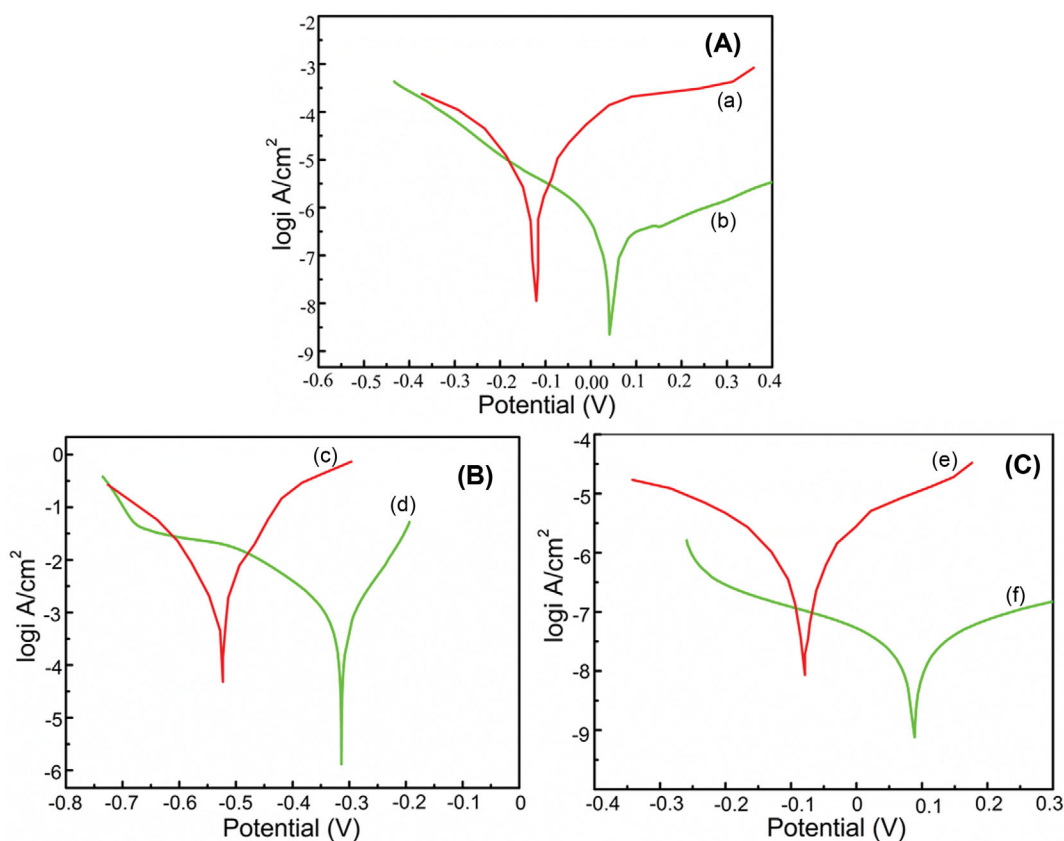

Fig. 14. Tafel plots obtained for (a), (c), (e) TiO$_2$-PVC/CS (b), (d), (f) TiO$_2$-TP-PVC/CS in (A) 1 M HCl (B) 1 M HCl (80 $^\circ$C) (C) rainwater medium.

Table 9. Tafel parameters obtained for bare TiO₂ and composited TiO₂ coating

Inhibitor system	Medium	E$_{corr}$ (V)	I$_{corr}$ (µA cm^2)	R$_p$ (Ω cm^2)	θ	IE (%)
TiO$_2$-PVC/CS	HCl	−0.121	71.3	6.87×10^2	-	-
TiO$_2$-PVC/CS	HCl at 80 $^\circ$C	−0.518	81.7	2.35×10^2	-	-
TiO$_2$-PVC/CS	Rainwater	−0.082	69.4	6.36×10^2	-	-
TiO$_2$-TP-PVC/CS	HCl	0.043	2.4	5.78×10^4	0.966	96.6
TiO$_2$-TP-PVC/CS	HCl at 80 $^\circ$C	−0.312	7.9	1.87×10^3	0.903	90.3
TiO$_2$-TP-PVC/CS	Rainwater	0.009	1.8	6.63×10^4	0.974	97.4

5-3. Anti-corrosive Performance of the Coatings

Anti-corrosive characteristics of the composited extract coated mild steel were analyzed by polarization and impedance analyses.

5-3-1. Tafel Polarization

Potentiodynamic polarization was conducted to explore the anti-corrosive characteristics of the coatings (Fig. 14). The results of polarization study of the coatings in 1 M HCl, 1 M HCl (80 °C) and rainwater medium are in Table 9. E_{corr} value of composited extract coated steel surface is significantly shifted to positive region, revealing the cathodic nature of the coating in all the studied environments. The I_{corr} value of the composited extract coating is remarkably low in all the mediums. The protective efficiency of the prepared coating followed the order: rain water>HCl>HCl (80 °C). The TiO$_2$-TP-PVC/CS had remarkably higher value for R_p, again confirmed its efficiency for corrosion inhibition. The IE of TiO$_2$-TP-PVC/CS in 1 M HCl (RT), 1 M HCl (80 °C) and rainwater mediums were given by 96.6%, 90.3% and 97.4%, respectively. The coating efficiency for corrosion inhibition decreased at elevated temperature, even though can ensure more than 90% IE [51].

5-3-2. EIS Analyses

The non-destructive, ac-impedance spectroscopic study evaluated the protective efficiency of the coating in terms of parameters such as R_{ct}, C_{dl} and R_s (Fig. 15). Fig. S3 represents the circuit diagram used to fit the Nyquist plot. The study also confirmed that the TiO$_2$-TP-PVC/CS exhibited excellent anti-corrosive performance in all the environments. The protective ability of the coating is incredible in rainwater medium, although the coating had excellent anti-corrosive performance in acidic environment too. The remarkable activity of TiO$_2$-TP-PVC/CS in rainwater medium is also evident from the polarization analyses. The coating excellence in rainwater medium could be interpreted in terms of anti-bacterial, anti-fungal and anti-oxidant activity of TP leaf extract in the coating [24,52]. The impedance parameters of TiO$_2$-TP-PVC/CS and TiO$_2$-PVC/CS in various environments are recorded in Table 10.
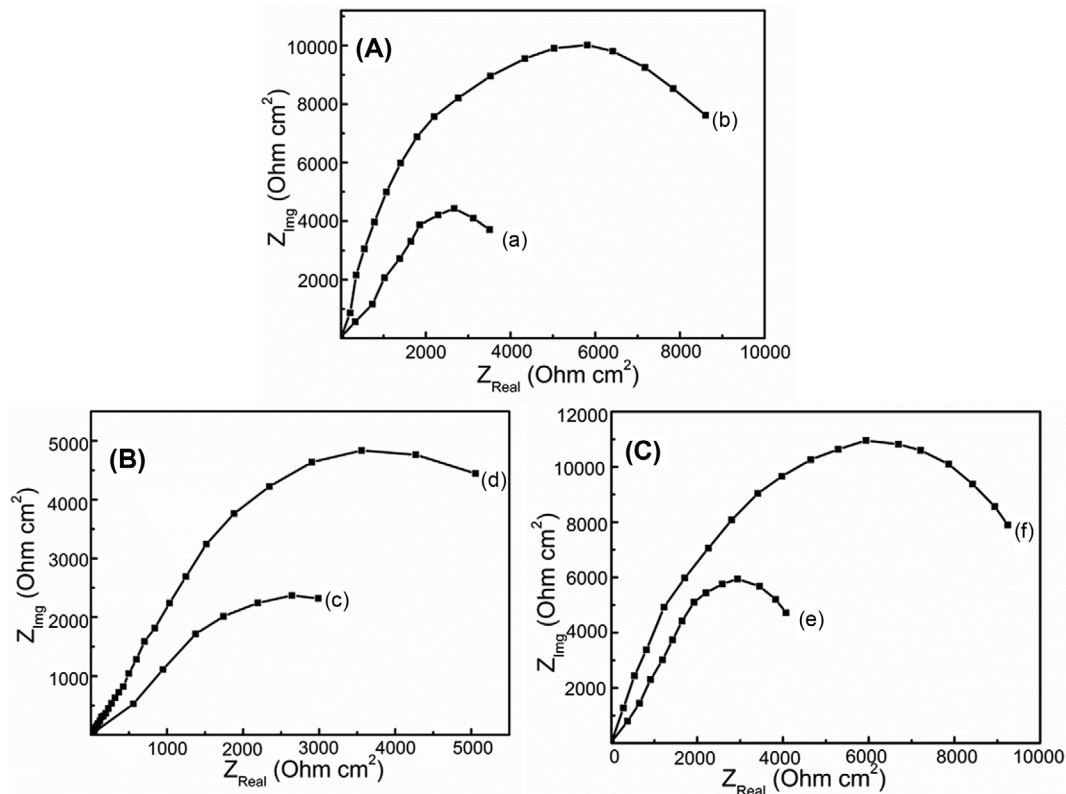

Fig. 15. Nyquist plots obtained for (a), (c), (e) TiO$_2$-PVC/CS; (b), (d), (f) TiO$_2$-TP-PVC/CS in (A) 1 M HCl (B) 1 M HCl (80 °C) (C) Rainwater medium.

Table 10. The impedance parameters obtained for TiO$_2$-TP-PVC/CS and TiO$_2$-PVC/CS in various environments

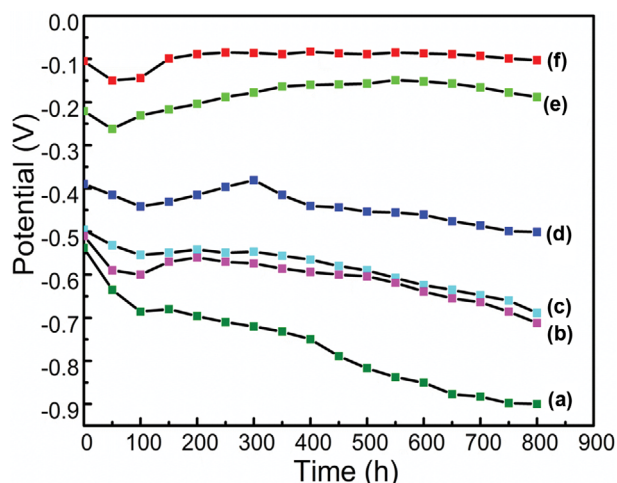| Inhibitor system	Medium	R_{ct} (Ω cm^{-2})	R_s (Ω cm^{-2})	C_{dl} (μF cm^2)	IE (%)
TiO$_2$-PVC	HCl	4,235	19	312	-
TiO$_2$-PVC	HCl at 80 °C	4,031	14	456	-
TiO$_2$-PVC	Rainwater	4,833	21	358	-
TiO$_2$-TP-PVC	HCl	11,723	52	6.3	97.9
TiO$_2$-TP-PVC	HCl at 80 °C	6,520	29	38	91.6
TiO$_2$-TP-PVC	Rainwater	12,351	64	5.2	98.5

Fig. 16. Open circuit potential of coatings in various environments (a) TiO$_2$-PVC/CS in 1 M HCl (80 $^{\circ}$C) (b) TiO$_2$-PVC/CS in 1 M HCl (RT) (c) TiO$_2$-PVC/CS in rainwater medium (d) TiO$_2$-TP-PVC/CS in 1 M HCl (80 $^{\circ}$C) (e) TiO$_2$-TP-PVC/CS in 1 M HCl (RT) (f) TiO$_2$-TP-PVC/CS in rain water medium.

5-3-3. Long Term Protective Efficiency of the Coating

Open circuit potential of the TiO$_2$-TP-PVC/CS and TiO$_2$-PVC/CS in 1 M HCl (RT), 1 M HCl (80 $^{\circ}$C) and rainwater medium was evaluated for 30 days and recorded in Fig. 16. TiO$_2$-TP-PVC/CS revealed the trend that OCP initially decreased and then increased after two or three days and then remained steady in all 1 M HCl (RT), 1 M HCl (80 $^{\circ}$C) and rainwater medium. Initial decrease in corrosion potential may be due to the entrance of electrolyte into the coating. TiO$_2$-TP-PVC/CS exhibited cathodic shift in all the studied environments. The cathodic shift is maximum in rainwater medium. In an acidic medium also, the coating demonstrated excellent cathodic behavior [24,53]. From the figure it is clear that the TiO$_2$-TP-PVC/CS is resistant to corrosion even up to 30 days. It can be seen that the more hydrophobic surfaces maintain a steady cathodic potential as compared to the hydrophilic surfaces. The observation is consistent with the fact that hydrophobicity hinders the interaction between the metal surface and the corrosive environment so that the metal surface resists corrosion and maintains a steady potential [25,50].

CONCLUSION

The present work explored the corrosion inhibition property of TP leaf extract. Also, it demonstrated the industrial significance of the plant extract by compositing it with TiO$_2$ to use it as an anticorrosive coating for mild steel. TiO$_2$, the primary constituent used to impart white color and opacity in the paint, here was composited with the extracted plant product. According to the result of EIS, the composite could arrest mild steel corrosion at the efficiency of 97.9%, 91.6%, and 98.5% in 1 M HCl, 1 M HCl at 80 $^{\circ}$C, and rainwater medium, respectively. The inhibition efficiency increased with an increase in the concentration of leaf extract. The efficiencies calculated by weight loss, Tafel, and EIS methods agreed with each other. Both anodic and cathodic polarization is altered

by the addition of leaf extract, confirming TP leaf extract as a mixed inhibitor. The corrosion inhibition efficiency of TP leaf extract decreases with increased temperature, implying the physisorption nature of adsorption. The free energy change of −13.18 kJ/mol confirmed that inhibition is affected by the physisorption of phytochemical constituents present in the extract. The Langmuir adsorption isotherm best explains the adsorption behavior of TP leaf extract. The proposed green inhibitor and TiO$_2$ composited leaf extract dominate other established green systems regarding their ease of availability, efficiency, long-term activity, and industrial utility.

DECLARATION OF INTERESTS

The authors declare that they have no known competing financial interests or personal relationships that could have appeared to influence the work reported in this paper.

CREDIT AUTHOR STATEMENT

Athira Krishnan: Conceptualization, Resources, Writing - original draft, Writing - review & editing

Data Availability Statement
All the data discussed are directly presented in tables and in graphical form in the manuscript and therefore they are immediately accessible.

NOTES

SUPPORTING INFORMATION

Additional information as noted in the text. This information is available via the Internet at http://www.springer.com/chemistry/journal/11814.

REFERENCES

1. I. H. Ali and M. H. A. Suleiman, *Int. J. Electrochem. Sci.*, **13**, 3910 (2018).
2. A. Krishnan, S. M. A. Shibli, S. Akashnath, A. Chithi, A. N. Vanikrishna and S. Vinayak, *Asian J. Chem.*, **29**, 2755 (2017).
3. A. S. Fouda, A. A. Nazeer and W. T. EI Behairy, *J. Bio. Tribo. Corros.*, **4**, 8 (2018).
4. T. K. Bhuvaneshwari, V. S. Vasantha and C. Jeyaprabha, *Silicon*, **10**, 1793 (2018).
5. A. Gopalakrishnan, B. J. Kariyil, R. John and P. T. A. Usha, *Phcog.*

Mag., **15**, 150 (2019).

6. H. Derfouf, Y. Harek, L. Larabi, W. J. Basirun and M. Ladan, *J. Adhesion Sci. Technol.*, **33**, 808 (2019).

7. M. Mobin, M. Basik and Y. El Aoufir, *J. Mol. Liq.*, **286**, 110890 (2019).

8. A. Miralrio and A. E. Vázquez, *Processes*, **8**, 942 (2020).

9. A. Krishnan and S. M. A. Shibli, *Anti-Corros Method M*, **65**, 210 (2018).

10. M. Mobin, M. Basik and J. Aslam, *Measurement*, **134**, 595 (2019).

11. A. Saxena, D. Prasad, R. Haldhar, G. Singh and A. Kumar, *J. Environ. Chem. Eng.*, **6**, 694 (2018).

12 D. Li, P. Zhang, X. Guo, X. Zhao and Y. Xu, *RSC Adv.*, **9**, 40997 (2019).

13. P. Tiwari, M. Srivastava, R. Mishra, G. Ji and R. Prakash, *J. Environ. Chem. Eng.*, **6**, 4773 (2018).

14. N. Raghavendra and J. I. Bhat, *Res. Chem. Intermed.*, **42**, 6351 (2016).

15. C. Verma, M. A. Quraishi, E. E. Ebenso and I. Bahadur, *J. Bio. Tribo. Corros.*, **4**, 33 (2018).

16. A. H. Al-Moubaraki, A. A. Al-Howiti, M. M. Al-Dailami and E. A. Al-Ghamdi, *J. Environ. Chem. Eng.*, **5**, 4194 (2017).

17. R. Sangeetha and N. Vedasree, *ISRN Pharmacol.*, **2012**, 1 (2012).

18. R. Rajamurugan, G. R. Shilpa, S. Kumaravel and R. Paranthaman, *Bio. Med. Rx.*, **1**, 248 (2013).

19. J. Rangani, A. Kumari, M. Patel, H. Brahmbhatt and A. K. Parida, *J. Food Biochem.*, **43**, 12731 (2019).

20. R. Gowtham, G. Umamaheswari, S. Bavani and V. Ambikapathy, *RJLBPCS*, **5**, 138 (2019).

21. H. S. Gadow and M. M. Motawea, *RSC Adv.*, **7**, 24576 (2017).

22. A. Saxena, D. Prasad, R. Haldhar, G. Singh and A. Kumar, *J. Mol. Liq.*, **258**, 89 (2018).

23. M. S. Suma, R. Basheer, B. R. Sreelekshmy, V. Vipinlal, M. Ameen Sha, P. Jineesh, A. Krishnan, S. R. Archana and S. M. A. Shibli, *Int. Biodeter. Biodegrad.*, **137**, 59 (2019).

24. K. K.Veedu, T. P. Kalarikkal, N. Jayakumar and N. K. Gopalan, *ACS Omega*, **4**, 10176 (2019).

25. A. Krishnan, B. Joseph, K. M. Bhaskar, M. S. Suma and S. M. A. Shibli, *Polym. Compos.*, **40**, 2400 (2019).

26. O. S. Shehata, L. A. Korshed and A. Attia, O. S. Shehata, L. A. Korshed and A. Attia, *Corrosion inhibitors, principles and recent applications*, United Kingdom: IntechOpen, London (2017).

27. X. Zheng, M. Gong, Q. Li and L. Guo, *Sci. Rep.*, **8**, 9140 (2018).

28. A. Dehghani, G. Bahlakeh and B. Ramezanzadeh, *Bioelectrochem*, **130**, 107339 (2019).

29. X. Wang, Y. Lingua, Q. Wang, Y. Wan, X. Huang and C. Jing, *Int. J. Electrochem. Sci.*, **13**, 5228 (2018).

30. Y. Qiang, S. Zhang, B. Tan and S. Chen, *Corros. Sci.*, **133**, 6 (2018).

31. M. P. Casaletto, V. Figà, A. Privitera, M. Bruno, A. Napolitano and S. Piacente, *Corros. Sci.*, **136**, 91 (2018).

32. K.S. Beenakumari, *Oriental J. Chem.*, **29**, 213 (2013).

33. S. A. Umoren, Z. M. Gasem and I. B. Obot, *Ind. Eng. Chem. Res.*, **52**, 14855 (2013).

34. T. Ibrahim and M. Habbab, *Int. J. Electrochem. Sci.*, **6**, 5357 (2011).

35. N. H. J. Al Hasan, H. J. Alaradi, Z. A. K. Al Mansor and A. H. J. Al Shadood, *Case Stud. Constr. Mater.*, **11**, e00300 (2019).

36. J. K. Odusote, D. O. Owalude, S. J. Olusegun and R. A. Yahya, *West Indian J. Eng.*, **38**, 64 (2016).

37. C. Verma, E. E. Ebenso, I. Bahadur and M. A. Quraishi, *J. Mol. Liq.*, **266**, 577 (2018).

38. A. A. S. Begum, R. M. A. Vahith, V. Kotra, M. R. Shaik, A. Abdel-gawad, E. M. Awwad and M. Khan, *Coatings*, **11**, 106 (2021).

39. S. K. Shukla, A. K. Singh, L. C. Murulana, M. M. Kabanda and E. E. Ebenso, *Int. J. Electrochem. Sci.*, **7**, 5057 (2012).

40. A. Saxena, V. Sharma, K. K. Thakur and N. Bhardwaj, *J. Bio. Tribo. Corros.*, **6**, 41 (2020).

41. A. Dehghani, G. Bahlakeh, B. Ramezanzadeh and M. Ramezanzadeh, *J. Ind. Eng. Chem.*, **84**, 52 (2020).

42. I. Ekere, O. Agboola and S. E. Sanni, *J. Phys.: Conf. Ser.*, **1378**, 022049 (2019).

43. M. B. Harb, S. Abubshait, N. Etteyeb, M. Kamoun and A. Dhouib, *Arabian J. Chem.*, **13**, 4846 (2020).

44. M. T. Saeed, M. Saleem, S. Usmani, I. A. Malik, F. A. Al-Shammari and K. M. Deen, *J. King Saud Univ. Sci.*, **31**, 1344 (2019).

45. E. Alibakhshi, M. Ramezanzadeh, G. Bahlakeh, B. Ramezanzadeh, M. Mahdavian and M. Motamedi, *J. Mol. Liq.*, **255**, 185 (2018).

46. P. M. Krishnegowda, V. T. Venkatesha, M. Punith Kumar, Krishne-gowda and S. B. Shivayogiraju, *Ind. Eng. Chem. Res.*, **52**, 722 (2013).

47. Z. Sanaei, M. Ramezanzadeh, G. Bahlakeh and B. Ramezanzadeh, *J. Ind. Eng. Chem.*, **69**, 18 (2019).

48. S. A. Umoren, Z. M. Gasem and I. B. Obot, *Ind. Eng. Chem. Res.*, **52**, 14855 (2013).

49. F. S. de Souza and A. Spinelli, *Corros. Sci.*, **51**, 642 (2009).

50. A. Krishnan, A. V. Krishnan, A. Ajith and S. M. A Shibli, *Surf. Interfaces*, **25**, 101238 (2021).

51. A. M. Abdel-Gaber, H. T. Rahal and F. T. Beqai, *Int. J. Ind. Chem.*, **11**, 123 (2020).

52. M. Tezeghdenti, L. Dhouibi and N. Etteyeb, *J. Bio. Tribol. Corros.*, **1**, 16 (2018).

53. K. Kalaiselvi, I. M. Chung, S. H. Kim and M. Prabakaran, *Anti-Corros. Method*, **65**, 408 (2018).